Catalytic oxidation of ethyl acetate and toluene over Cu-Ce-Zr supported ZSM-5/TiO2 catalysts

Article *in* RSC Advances · January 2016

DOI: 10.1039/C6RA06421C

7 authors, including:

Baojuan Dou
Tianjin University of Science and Technology
25 PUBLICATIONS **500** CITATIONS
SEE PROFILE

Liu Jingge
Chinese Academy of Sciences
4 PUBLICATIONS **6** CITATIONS
SEE PROFILE

Hao Qinglan
Tianjin University of Science and Technology
29 PUBLICATIONS **171** CITATIONS
SEE PROFILE

Feng Bin
Chinese Academy of Sciences
20 PUBLICATIONS **183** CITATIONS
SEE PROFILE

RSC Advances

PAPER

Cite this: *RSC Adv.*, 2016, **6**, 53852

Catalytic oxidation of ethyl acetate and toluene over Cu–Ce–Zr supported ZSM-5/TiO_2 catalysts

Dou Baojuan,[a] Li Shumin,[b] Liu Deliang,[b] Zhao Ruozhu,[b] Liu Jingge,[b] Hao Qinglan*[b] and Bin Feng*[c]

Received 10th March 2016
Accepted 18th May 2016

DOI: 10.1039/c6ra06421c

www.rsc.org/advances

Copper–cerium–zirconium catalysts loaded on ZSM-5/TiO_2 (denoted as CCZ/Z and CCZ/T) were prepared and characterized in this investigation and the catalytic behaviors of VOCs over the catalysts were determined. It is shown that the low-temperature activities of ethyl acetate and toluene oxidation over the CCZ/T catalyst are obviously higher than that over the CCZ/Z catalyst. Compared with CCZ/Z, the force between the metal oxides and the support TiO_2 is weaker and TiO_2 can provide some lattice oxygen. The greater number of oxygen vacancies, together with more Cu^+ species in CCZ/T increases the mobility of atomic oxygen anions, which can inhibit by-product formation and enhance catalytic activity effectively. Moreover, the larger pore size of CCZ/T is beneficial for the diffusion of reactants and products. The analysis of intermediate species and the Mars–van Krevelen mechanism well explain the superior oxidation performances of ethyl acetate and toluene on CCZ/T. Both CCZ/Z and CCZ/T show superior stability for the catalytic removal of ethyl acetate and toluene at their complete conversion temperatures, which contribute to the positive effects of the Ce–Zr promoters on the copper species and support.

1 Introduction

Volatile organic compounds (VOCs) are a series of important environmental pollutants that originate from petroleum refineries, solvent cleaning, fuel storage and motor vehicles.[1–3] VOCs not only cause terrible environmental problems such as photochemical smog, but are also great threats to human health due to their carcinogenic, mutagenic, and teratogenic nature.[4–6] In addition, VOCs are responsible for the formation of secondary particulate matter in the atmosphere, which contribute to haze formation.[7] Therefore, it is very desirable to completely convert VOCs into CO_2 and H_2O.[8]

Catalytic oxidation is one of the most efficient and environmentally friendly technologies for VOCs removal. More importantly, low temperatures (generally around 250–500 °C) are required, thus preventing the formation of undesirable intermediate products.[9–15] The commonly used catalysts for VOCs removal are noble metals and transition metal oxides. Noble metals have higher activity compared with transition metal oxides. However, attention has been given to transition metals due to the limited availability and high cost of noble metals. A common feature of these materials is the presence of multiple oxidation states of the transition metal in the structure, which result in the ability of the cation to undergo reversible oxidation and reduction under reaction. Compared with other transition metal oxides, CuO is one of the most active catalysts for the elimination of various VOCs.[16–20] However, the catalytic activity of transition metal oxides is still not as high as noble catalysts. Numerous studies were undertaken to improve the catalytic performance of transition metals by modifying the catalyst support, adding promoters and forming a solid solution of the catalyst. For example, a CeO_2 and/or ZrO_2 promoter was intensively studied to improve the oxygen storage capacity, redox properties, thermal stability and catalytic performances in VOCs elimination.[21–23]

However, unsupported metal oxidation catalysts display poor thermal stability, low specific surface areas and weak mechanical strength, which severely limit their use in practical industrial applications. Fortunately, the function of a catalytic support can offset this defect.[24] Bin *et al.*[25] found that CO self-sustained combustion was achieved over a Cu–Ce/ZSM-5 catalyst with a CO concentration ≥5 vol%, due to the formation of Cu^{2+} ions incorporated into cerium oxides, which are more reducible than the copper clusters on the ZSM-5 support. A previous study demonstrated that Cu–Zr/ZSM-5 catalysts exhibited excellent catalytic activity for the selective catalytic reduction (SCR) of NO.[26] Recently, Ce/Zr promoted copper/ZSM-5 catalysts have been found to have excellent activity and stability for VOCs oxidation.[27] Moreover, the TiO_2 supported metal oxides have been widely used for the past few decades. No

[a]*College of Marine & Environmental Sciences, Tianjin University of Science & Technology, Tianjin 300457, China*

[b]*College of Chemical Engineering & Materials Science, Tianjin University of Science & Technology, Tianjin 300457, China. E-mail: haoqinglan@tust.edu.cn*

[c]*State Key Laboratory of High-Temperature Gas Dynamics, Institute of Mechanics, Chinese Academy of Science, Beijing 100190, PR China. E-mail: binfeng@imech.ac.cn*

characteristic peaks associated with either copper, cerium/zirconium oxides are observed for Cu–Ce–Zr/TiO_2 catalysts, and this indicates that the metal oxides species are formed in the nanometer size range and well dispersed on the surface of the TiO_2 support, which exhibit high NH_3-SCR activity in NO_x abatement over a wide temperature range.[28] However, the use of Ce/Zr promoted copper/TiO_2 catalysts in the VOCs oxidation process has seldom been reported. In particular, the comparison of catalytic behavior and reaction pathway of VOCs between Cu–Ce–Zr/ZSM-5 and Cu–Ce–Zr/TiO_2 is of great significance and should be further explored.

In the present study, toluene and ethyl acetate, which are two types of typical saturated aliphatic hydrocarbons and aromatics that vastly exist in industrial processes, were adopted as probe pollutants to evaluate the catalytic performances over Cu–Ce–Zr metal oxides supported on ZSM-5/TiO_2. The correlations between catalyst activity and structural characteristic, dispersion, and reduction adsorption/desorption behaviors are investigated *via* extensive characterization. The focus is to explore the differences between ethyl acetate and toluene degradation over CCZ/Z and CCZ/T catalysts, in an attempt for complete oxidation of VOCs by examining the effect of the ZSM-5/TiO_2 support and to develop more efficient catalyst formulations for the catalytic oxidation of VOCs.

2 Experimental

2.1 Catalyst preparation

H/ZSM-5 with an atomic Si/Al ratio of 25 was supplied by Nankai University and the TiO_2 support was pure anatase titanium dioxide, which was obtained commercially from Degussa. The supported catalysts were prepared *via* the wet impregnation method. Copper nitrate, cerium nitrate and zirconium nitrate were dissolved in deionized water and mixed with 20 g H-ZSM-5/TiO_2 powder at room temperature until the water evaporated. The resulting precursor was dried at 105 °C for 24 h in air and then calcined at 550 °C for 4 h. The copper content of the two catalysts were fixed at 4 wt% and the molar ratio of Cu/(Ce + Zr) was 1 : 1. The catalysts were denoted as CCZ/Z and CCZ/T. To evaluate catalytic activity, catalyst pellets were pressed under the pressure of 20 MPa, then granulated and screened to a size of 20–40 mesh.

2.2 Catalyst characterization

N_2 adsorption/desorption isotherms were measured at −196 °C using an Autosorb-Iq-MP instrument (Quantachrome). The samples were degassed at 300 °C for 4 h before measurement. The BET surface area of the samples was obtained according to the Brunauer–Emmett–Teller (BET) method and the microporous pore size distribution was achieved using the Horvath–Kawazoe (HK) theory and the mesoporous pore size distribution was calculated using the Barrett–Joyner–Halenda (BJH) equation. X-ray diffraction (XRD) patterns were obtained on an XD-3-automatic (PERSEE) equipped with a multi-crystal X-ray diffractometer using Cu Kα radiation in the 2θ range of 5–80° (scanning rate of 4° min^{-1}) and a step size of 0.02°. Ultraviolet-visible diffuse reflectance spectra (UV-Vis DR) were obtained in the range of 200–1000 nm at room temperature on a Perkin Elmer Lambda 750 UV-Vis spectrophotometer with an integration sphere diffuse reflectance attachment. X-ray photoelectron spectroscopy (XPS) experiments were conducted on a Perkin-Elmer PHI-1600 ESCA spectrometer using an Mg Kα X-ray source. The binding energy (BE) was calibrated based on the line position of C 1s (285 eV). Fourier transform infrared (FTIR) spectra of the catalysts in KBr pellets were scanned in the range between 4000 and 400 cm^{-1} on a TENSOR27 spectrometer (Germany-Bruker). Temperature-programmed reduction experiments with hydrogen (H_2-TPR) were investigated on a PCA-140 instrument (Bolider) with a thermal conductivity detector (TCD). 200 mg of each sample was first pretreated in a quartz U-tube under an Ar stream (30 mL min^{-1}) from room temperature to 500 °C for 60 min at a rate of 20 °C min^{-1}. The samples were then purged from 100 °C to 800 °C at 10 °C min^{-1} in 5% H_2/Ar with a flow rate of 50 mL min^{-1}. Temperature-programmed desorption of ammonia (NH_3-TPD) was also carried out on the abovementioned PCA-140 instrument (Bolider). Prior to the adsorption experiment, the sample (~200 mg) was first pretreated under the same condition of H_2-TPR. The adsorption step was performed by admitting 5% NH_3/Ar (50 mL min^{-1}) at 100 °C to saturation. Subsequently, the sample was exposed to a flow of Ar for 30 min at 100 °C to remove reversibly and physically bound ammonia from the catalyst surface. Finally, desorption was carried out from 100 °C to 800 °C at a rate of 10 °C min^{-1}.

2.3 Catalyst tests

Catalytic performance was investigated in a continuous-flow fixed-bed reactor at atmospheric pressure, which comprised a stainless steel tube that was filled with the catalyst. Streams with the VOC were produced by bubbling air through VOC saturators. Then, the gas containing the VOC was further diluted with another air stream to the required concentration before reaching the fixed-bed. The gas flow rates of the two branches were metered by mass flow controllers.

In each test, 0.8 g of catalyst (20–40 mesh) was placed in the middle of the fixed-bed and the total flow rate was 400 mL min^{-1}, which corresponds to a space velocity of 24 000 h^{-1}, and the concentration of ethyl acetate and toluene in the air feed was 1000 ppm and 750 ppm, respectively. The fixed-bed temperature was first increased to 80 °C with the passing gas stream and stabilized for 30 min. The effluent gas composition was analyzed *via* a gas chromatograph (GC-7900, Shanghai Tianmei Co., China) equipped with an FID (HP-5) for analysis of the VOCs and by-products quantitatively.

3 Results and discussion

3.1 Textural properties

Fig. 1A and B show the N_2 adsorption and desorption isotherms and the corresponding pore size distributions of the CCZ/Z and CCZ/T catalysts. The CCZ/Z and CCZ/T catalysts display typical I and IV shape isotherms with the P/P_0 of the material according

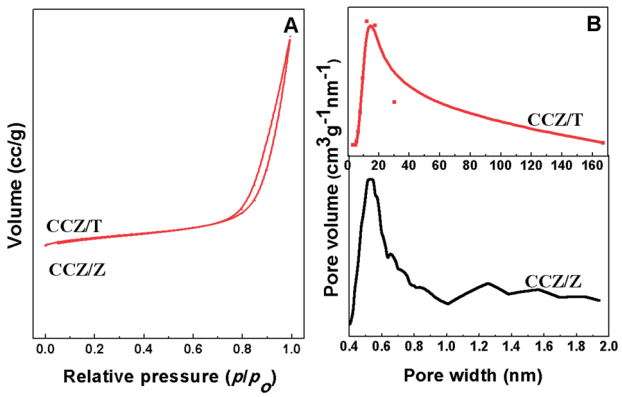

Fig. 1 N_2 adsorption/desorption isotherms curves (A) and pore size distributions (B) of CCZ/Z and CCZ/T.

to the IUPAC classification, respectively. The pore size distribution curve of CCZ/Z exhibits one single narrow peak centered at 0.4–0.8 nm (Fig. 1B), which suggests good micropore homogeneity, whereas the pore size of CCZ/T (6–120 nm) is much higher than that of CCZ/Z. In addition, the specific surface area of the CCZ/Z catalyst (339 $m^2\ g^{-1}$) is much higher than that of CCZ/T (49 $m^2\ g^{-1}$).

3.2 XRD measurement

The XRD powder patterns of CCZ/Z and CCZ/T compared with the support of ZSM-5 and TiO_2 are shown in Fig. 2. CCZ/Z shows the typical diffraction peaks at $2\theta = 7.5°$, 8.1°, 23.1° and 24.5°, which represent the (011), (200), (051) and (303) crystal structure planes, respectively.[26] The main diffraction peaks of crystalline CCZ/T appear at $2\theta = 25.3°$, 38.4°, 48.1° and 54.0°, and these diffraction angles are consistent with the fluorite structure of TiO_2 (101), (004), (112), (200) and (105) crystal structure planes, respectively.[28] No diffraction peaks attributed to metal oxides are observed, which suggests that the copper, cerium and zirconium species are homogeneously dispersed on the ZSM-5 and TiO_2 supports. The abovementioned results indicate that the catalysts still maintain their structure after wet impregnation.

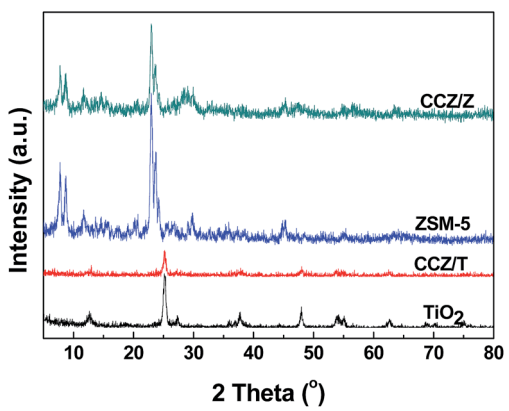

Fig. 2 XRD diffraction spectra for CCZ/Z, CCZ/T and the supports of ZSM-5 and TiO_2.

3.3 UV-Vis spectroscopy

The UV-Vis diffuse reflectance spectra of the CCZ/Z and CCZ/T samples are plotted in Fig. 3. The CCZ/Z and CCZ/T catalysts present two adsorption bands at 200–500 and 600–1000 nm, respectively. For CCZ/Z, the two adsorption bands can be well fitted by four peaks. The peak at 200 nm can be attributed to the oxygen-to-metal charge transfer related to the Cu^+/Cu^{2+} ions[13] and the peak at 284 nm is assigned to $O^{2-} \rightarrow Ce^{4+}$ charge transfer transitions and inter band transitions.[30] The weak peak at 460 nm can be assigned to the transitions of Cu^{2+} in the tetragonal oxygen configuration,[13,31] which can be attributed to the formation of well dispersed copper species on the surface of ZSM-5. This result is in conformity with the characterization results obtained from the XRD analysis. The absorption band at 700–1000 nm is related to the transitions of Cu^{2+} in the octahedral oxygen configuration, which is more or less tetragonally distorted, and corresponds to the CuO phase.[13]

For CCZ/T, five adsorption peaks at 201, 266, 327 nm, and two broad bands at 200–550 and 500–1000 nm were discovered by peak-fit processing. The adsorption peak at 327 nm, which corresponds to the $O^{2-} \rightarrow Ce^{3+}$ charge transition, was clearly observed. It is reported that the existence of Ce^{3+} in CeO_2 implies the formation of an oxygen vacancy.[5] Obviously, the Ce^{3+} content in the CCZ/T catalyst is higher than that in the CCZ/Z sample, which suggests that the former provides more oxygen vacancies than the latter. The position and intensity of these adsorptions are in direct linear relationship with the mount of surface electrons, because the enhanced concentration of oxygen vacancies in composite oxide systems forms a defect band which further changes the energy of the conduction band.[23] It can be observed from Fig. 3 that the peak intensity of the adsorption band and its position for CCZ/T are obviously higher than that for CCZ/Z, thus further indicating that CCZ/T possesses more oxygen vacancies.

3.4 XPS analysis

The CCZ/Z and CCZ/T catalysts were analyzed *via* XPS to obtain their surface compositions and chemical states, as shown in Fig. 4 and Table 1. Fig. 4A depicts the XPS spectra in the Cu 2p region for the CCZ/Z and CCZ/T catalysts. The CCZ/Z sample is

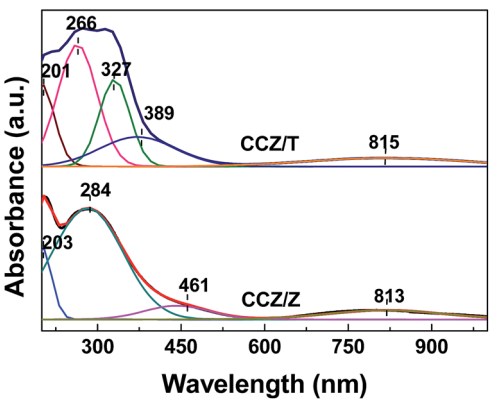

Fig. 3 UV-Vis diffuse reflectance spectra of the CCZ/Z and CCZ/T catalysts.

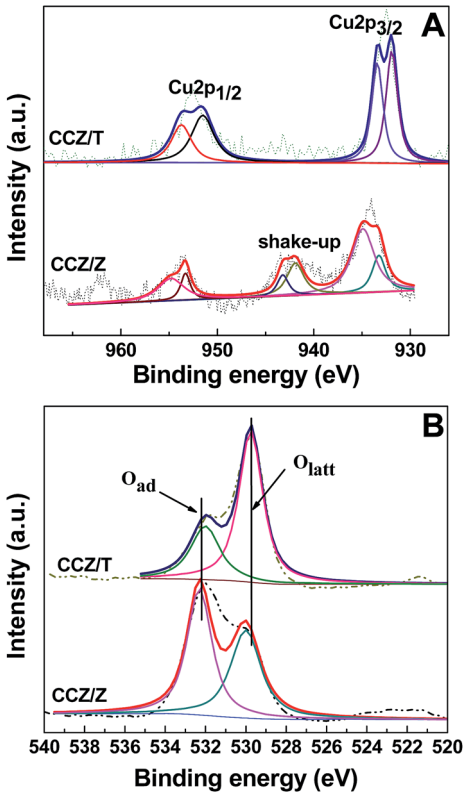

Fig. 4 XPS narrow spectra of Cu 2p (A) and O 1s (B) for the CCZ/Z and CCZ/T catalysts.

characterized by two main peaks of Cu $2p_{1/2}$ (952.5–955 eV) and Cu $2p_{3/2}$ (930–935 eV), along with shake-up satellite peak centered at 937.5–947.5 eV.[4,5] According to relevant studies,[4,5,26,27,29] the Cu $2p_{3/2}$ binding energy at *ca.* 933–934.2 eV, in combination with the appearance of shake-up peaks are typical characteristics of Cu^{2+}. A lower binding energy at *ca.* 932–933 eV is characteristic of further reduced copper species, mainly Cu^{+}. These results suggest the coexistence of Cu^{+} and Cu^{2+} ions in the CCZ/Z catalyst,[4,5,27] whereas the lower binding energy at *ca.* 932–933 eV and the absence of the shake-up peak are characteristics of further reduced copper species, mainly Cu^{+}. For the CCZ/T catalyst, it is evident that the copper is mostly in the Cu^{+} oxidation state (see Table 1).

The high resolution XPS spectra of the CCZ/Z and CCZ/T catalysts for O 1s are shown in Fig. 4B, after deconvolution into two different oxygen species. According to the literatures, the higher binding energy at 531.6 eV is attributed to the lattice oxygen (O_{latt}) associated with copper, cerium and zirconium metal oxides, whereas the lower binding energy at 529.6 eV is ascribed to absorbed oxygen (O_{ads}).[25,27,28] The quantitative result (see Table 1) reveals that the $O_{latt}/(O_{latt} + O_{ads})$ ratio of the CCZ/T catalyst is markedly higher than that of CCZ/Z, which indicates that TiO_2 provides some lattice oxygen.[28]

Table 1 Surface species of the CCZ/Z and CCZ/T catalysts

Catalyst	Cu^{2+}/Cu^{+}	$O_{latt}/(O_{latt} + O_{ads})$ (%)
CCZ/Z	2.96	0.14
CCZ/T	—	0.52

3.5 FT-IR analysis

The functional groups of the samples were determined using FT-IR and the spectra of the fresh and used catalysts are shown in Fig. 5. For fresh CCZ/Z, the peaks located at 513, 819 and 859 cm^{-1} represent the asymmetrical stretching vibration of Si–O–Si and the band at around 949 cm^{-1} is due to the asymmetrical stretching vibration of SiO_4. The feature peaks of fresh CCZ/T at low 1000 cm^{-1} is discernible and is ascribed to the flexural vibration of O–Ti–O, and the peaks at 1079 and 1127 cm^{-1} are attributed to the characterized vibration of Ti–O. Compared with the fresh CCZ/Z, the presence of the absorption peak at 1061 cm^{-1} after removal of ethyl acetate is attributable to the C–OH bond deformation vibration, thus illustrating the generation of ethanol on the catalyst surface.[4,27] However, no new spectrum was detected for the used CCZ/T after ethyl acetate removal, which proved that there was no intermediate species over the catalytic surface. The bands in the range of 860–800 cm^{-1} and 800–750 cm^{-1} are assigned to the feature adsorption peaks for mono-substituted phenyl. With respect to the used CCZ/Z for toluene removal, the peak at 1665 cm^{-1} is assigned to the stretching vibration of C=O, and the band in the range of 541–451 cm^{-1} is ascribed to the flexural vibration of C=O, which suggest the formation of benzaldehyde on the catalyst surface.[34] The feature peaks at around 1719, 1266 and 947 cm^{-1} are attributed to the flexural vibration of –OH coupling with the stretching vibration of C=O, thus indicating the generation of benzoic acid on the surface of CCZ/T.[34]

3.6 H_2-TPR

The reducibility of the samples was explored *via* H_2-TPR studies. Fig. 6 displays the H_2-TPR results obtained over CCZ/T and CCZ/T, together with ZSM-5/TiO_2 supported copper catalysts (Cu/Z and Cu/T). As shown in Fig. 6, the Cu/Z catalyst exhibits three main reduction peaks, which are denoted as α, β and γ. The α peak is attributed the reduction of well

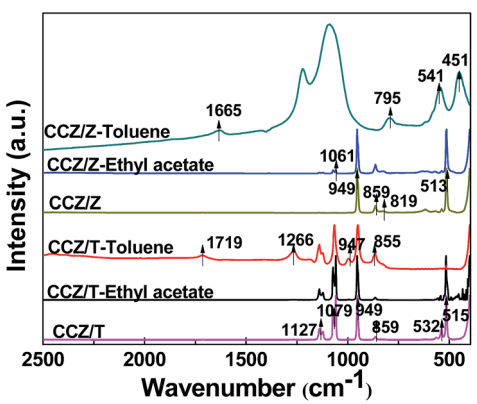

Fig. 5 FT-IR profiles of the fresh and used CCZ/Z and CCZ/T catalysts.

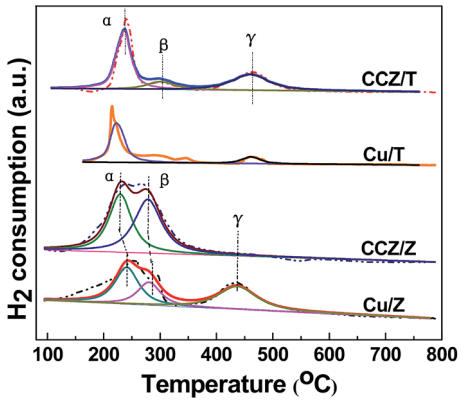

Fig. 6 H_2-TPR profiles of the CCZ/Z and CCZ/T catalysts.

dispersed copper species on the ZSM-5 support, and the β peak is associated with the reduction of the copper oxide adhering to the external surface of zeolite crystallites, whereas the γ peak is generally proposed as the reduction of the bulk copper oxide.[32,33] Compared with Cu/Z, the α and β peaks of CCZ/Z shift to a lower temperature; moreover, the γ peak disappears with the Ce and Zr incorporation. When copper, cerium and zirconium species are loaded, surface shell reduction is facilitated and these peaks can slightly shift to lower temperatures. The Cu/T catalyst exhibits two reduction peaks. The α peak (200 °C) generally results from the reduction of the copper species dispersed on the TiO_2 support and the γ peak (440 °C) is due to the interactions between CuO and TiO_2, and oxygen reduction on the TiO_2 surface.[27] Upon the addition of zirconium and cerium, the position of the reduction peak for CCZ/T presents no shift, which implies the weak force between the metal oxides and the support TiO_2. Moreover, partial copper species are incorporated into the vacant sites of zirconium oxides or cerium oxides to form a coordinated surface structure with the capping oxygen,[30,31] which corresponds to the β peak (270 °C).

The total H_2 consumption is summarized in Table 2. It is worth noting that the H_2 consumption of the α and β peaks for the CCZ/Z and CCZ/T catalysts increase with the incorporation of Ce and Zr. The disappearance of H_2 consumption of the γ peak for CCZ/Z is due to the incorporation of zirconium and cerium into the catalyst, which promotes the dispersion of the copper species. In this study, the total amount of H_2 consumption increases from 61 to 73.9 mol g^{-1} with the incorporation of Ce–Zr into Cu/Z. The total amount of H_2 consumption of the CCZ/T catalyst is significantly higher than that of Cu/T, which suggests that the Cu species were incorporated into vacant sites of the cerium oxides to form a coordinated surface structure. Combining with the XRD results, Cu and Zr ions incorporated in the cubic lattice of Ce form a homogeneous Cu–Ce–Zr–O solid solution.[27] It is also worth mentioning that the increment of total amount of H_2 consumption for CCZ/T is obviously more than that for CCZ/Z, thus indicating that the support TiO_2 provides some oxygen species.

Table 2 H_2 consumption of the CCZ/Z and CCZ/T catalysts

	H_2 consumption (mol g^{-1})			
Catalyst	α-Peak	β-Peak	γ-Peak	Total
Cu/Z	23.3	14	23.8	61
CCZ/Z	35.0	38.9	—	73.9
Cu/T	14.3	—	3.3	17.6
CCZ/T	21.3	5.8	15.4	42.5

3.7 Temperature-programmed desorption of ammonia

The acid properties of the catalytic materials were analyzed *via* the TPD of ammonia. The NH_3-TPD profiles of CCZ/Z, CCZ/T, and the ZSM-5 and TiO_2 supports are shown in Fig. 7. As shown in Fig. 7A, the NH_3-TPD profile of ZSM-5 displays two desorption peaks. The low-temperature peak is assigned to weakly bound NH_3 and the high-temperature peak is attributed to the NH_3 adsorbed on the strong acid sites of Si–OH–Al. Upon the incorporation of copper, cerium and zirconium, the uptake of weakly bound NH_3 decreases; moreover, the desorption peak of the strong acid sites shifts to a high temperature, which mainly originates from metal oxide nanoclusters.[26] As shown in Fig. 7B, the NH_3-TPD profile of TiO_2 presents one broad desorption peak in the temperature range of 50–400 °C. The desorption peak at 80–200 °C is associated with weakly bound NH_3 and the desorption peak at around 400 °C is assigned to NH_3 bound to strong acid sites. The desorption peak of strong acid sites shifts to a low temperature with the incorporation of copper, cerium and zirconium for the CCZ/T catalyst, thus suggesting that a low temperature is easy to strip the adsorbate after the addition of metal oxides. In addition, it can be observed that the intensity of the total acidity, which is lower for pure TiO_2, significantly increases upon the addition of copper, cerium and zirconium.

3.8 Catalyst performances

The investigation of the catalytic performances of CCZ/Z and CCZ/T was conducted in a fixed-bed reactor for the removal of ethyl acetate and toluene. Fig. 8A and B shows the catalytic behavior of the CCZ/Z and CCZ/T catalysts toward ethyl acetate and toluene oxidation. It can be observed that the more active

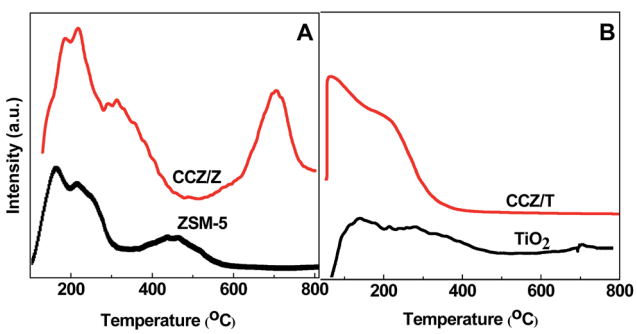

Fig. 7 NH_3-TPD profiles of the CCZ/Z and CCZ/T catalysts.

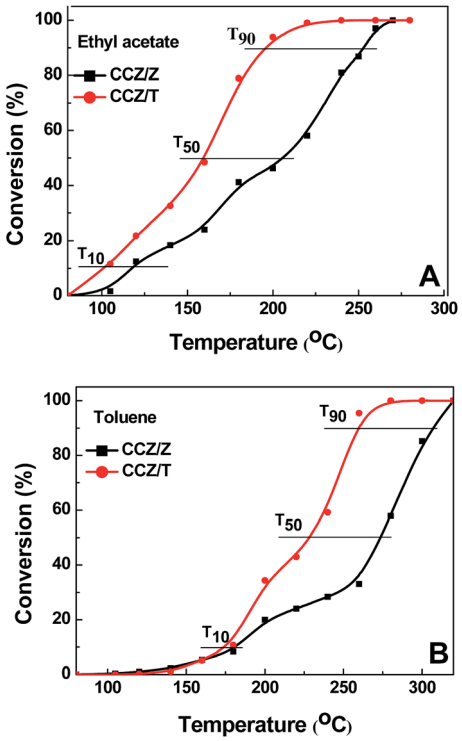

Fig. 8 Conversion of the CCZ/Z and CCZ/T catalysts in the oxidation of ethyl acetate (A) and toluene (B) as a function of temperature.

catalyst is CCZ/T with full combustion of ethyl acetate and toluene being achieved at 258 and 280 °C, respectively. For the catalytic oxidation of ethyl acetate over CCZ/T, the onset temperature (T_{10}) is as low as 102 °C, which is lower by 58 °C compared with unsupported Cu–$Ce_{1-x}Sm_xO_\delta$ catalysts that have a T_{10} of 160 °C,[4] and the complete conversion temperature is lower by 22 °C compared with Cu–Ce/SiO_2 (280 °C).[24] The T_{90} of toluene removal over the CCZ/T catalyst is 259 °C, which is lower than that of most reported catalysts.[5]

From the characterization results, it can be concluded that the pore size distribution is obviously the important factor that decides catalytic activity. Compared with CCZ/Z, the larger pore size assigned to mesopores and macropores in CCZ/T is beneficial for the adsorption, desorption and diffusion of VOCs. In addition, the presence of abundant oxygen vacancies on the CCZ/T surface facilitates the activation of more oxygen molecules to active oxygen adspecies, which consequently enhance its catalytic activity.

Combined with the results of XPS, CCZ/T, which is mostly in the Cu^+ state on the support surface, exhibits better catalytic behavior. Cu^+ can generate more ion-defects on the support surface because of charge compensation in metal oxidation, and consequently, it can improve the catalytic activity. Ce^{3+} and Cu species are indicative of the redox equilibrium ($Ce^{4+} + Cu^+ \leftrightarrow Ce^{3+} + Cu^{2+}$) shifting to right, which increases the mobility of lattice oxygen. On the other hand, according to the XPS and H_2-TPR results, the TiO_2 support provides some lattice oxygen. Moreover, the Cu and Zr ions incorporated in the cubic lattice of Ce form a homogeneous Cu–Ce–Zr–O solid solution, which allows numerous oxygen vacancies thus increasing the mobility of atomic oxygen anions, which may accelerate the ability of stored/released oxygen for the CCZ/T catalyst.

A small portion of ethyl acetate can be converted to intermediate species, such as ethanol, acetaldehyde and acetic acid, at low temperatures. Fig. 9 shows the intermediates yield of the catalytic oxidation of ethyl acetate (Fig. 9A) and toluene (Fig. 9B) over CCZ/Z and CCZ/T as a function of reaction temperature. In this study, ethanol is a unique intermediate product in the removal of ethyl acetate over CCZ/Z (Fig. 9A). However, it should be noted that no intermediate was discovered for catalytic the oxidation of ethyl acetate on CCZ/T, which is in conformity with the results obtained from the FT-IR analysis. It can be observed that the variation of the ethanol yield for ethyl acetate over CCZ/Z initially increases remarkably and then reaches a maximum before a rapid decrease and even disappears with a further increase of temperature to 250 °C. Combined with the FT-IR results, it can be observed from Fig. 9B that very small amounts of benzaldehyde and benzoic acid are formed at a lower temperature during toluene removal over CCZ/Z and CCZ/T, respectively. However, the intermediates of benzaldehyde and benzoic acid can be further completely oxidized with a temperature higher than 250 °C. Even though the types of intermediate products for CCZ/Z and CCZ/T catalysts are different, the results exhibit the same trend, which initially increases remarkably and then reaches a maximum at 180 °C before decreasing and even disappearing at 255 °C. It is worth mentioning that the yield of benzaldehyde is slightly higher than benzoic acid at the same reaction temperature. This can be

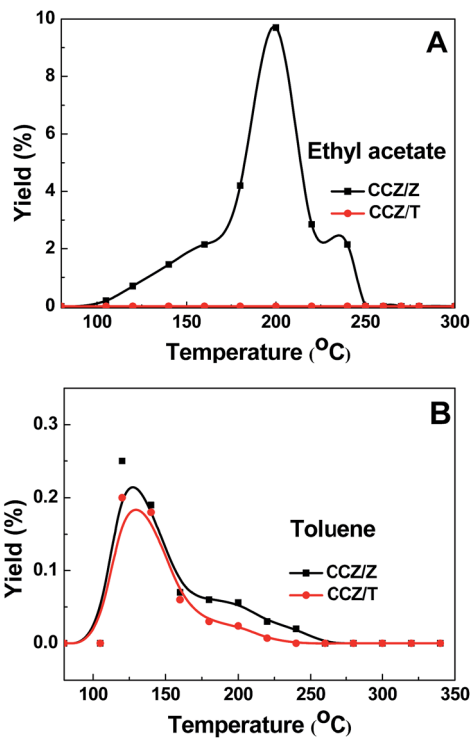

Fig. 9 Yield of intermediate as a function of reaction temperature for ethyl acetate (A) and toluene (B) over the CCZ/Z and CCZ/T catalysts.

explained by the results from UV-Vis, which show that CCZ/T possesses more oxygen vacancies and increased mobility of atomic oxygen anions, which may inhibit intermediate product formation in favor of CO_2.

The proposed catalytic oxidation reaction pathways of ethyl acetate and toluene are displayed in Fig. 10. The catalytic oxidation reactions occur with electronic transfers among the Cu–Ce–Zr based catalysts, reactants and intermediate species formed. For most catalytic oxidations occurring over Cu–Ce–Zr based catalysts, the Mars–van Krevelen mechanism well explains the oxidation reaction,[35] wherein organic molecules are primarily oxidized by the lattice oxygen of metal oxides. The Mars–van Krevelen mechanism assumes that in the first step (1), the oxygen from the catalyst oxidizes the reactant from the gas phase and produces reduced active sites on the catalyst surface and oxidation products that immediately leave the catalyst surface. In the second step (2) the catalyst is reoxidized by oxygen from the gas phase.[1] First, a small portion of gas phase VOCs can be oxidized to CO_2 and H_2O by the oxygen from the support on account of the excellent oxygen storage capability of CeO_2 and activated absorbed oxygen, while the majority of VOCs are oxidized by lattice oxygen released from the catalysts oxides. Simultaneously, oxygen vacancies on the catalyst surface are released and the metal centers (copper and cerium species) are reduced. Second, the oxygen vacancies are supplemented by oxygen from the gas phase when the catalyst is reoxidized. In this study, it is deduced that the activation of ethyl acetate and toluene over the CCZ/Z and CCZ/T catalysts occurs by the abstraction of the H atoms from the weakest C–H bonds, with a simultaneous reduction of the surface sites and successive formation of surface hydroxide ions.[1,5] The active oxygen preferentially extracts the H atoms from the weakest C–H bonds in ethyl acetate and toluene molecules and therefore more lattice oxygen species in the catalyst can facilitate the oxidation of ethyl acetate and toluene. In addition, the presence of oxygen vacancies promotes the activation of oxygen molecules to active oxygen species. In comparison to CCZ/Z (Fig. 10A), CCZ/T (Fig. 10B) provides more reactive oxygen species owing to more lattice oxygen partially provided by TiO_2

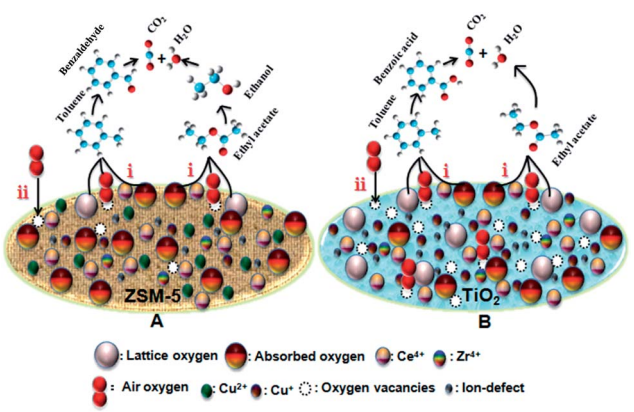

Fig. 10 Schematic of VOCs oxidation mechanism over the CCZ/Z (A) and CCZ/T (B) catalysts.

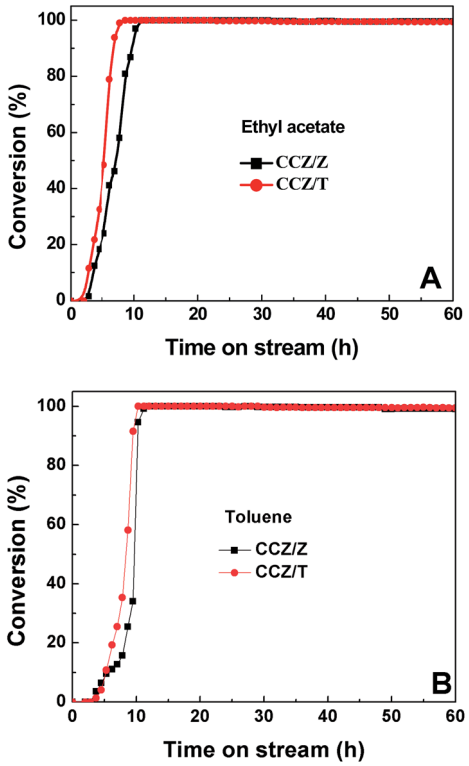

Fig. 11 Stability of the CCZ/Z and CCZ/T catalysts at their complete conversion temperatures as a function of time on stream.

and the weak force between the support and the metal oxides, which can oxidize more VOCs molecules rapidly.

The stability of the CCZ/Z and CCZ/T catalysts at complete conversion temperature is displayed in Fig. 11. In Fig. 11A, at the reaction temperature of complete conversion, it is observed that CCZ/Z and CCZ/T could retain high stability for ethyl acetate removal of around 99.7% without noticeable activity loss throughout the 60 h test. Similarly, the conversion of toluene over CCZ/Z and CCZ/T always remained above 99% at the temperature of complete conversion (320 °C for CCZ/Z and 280 °C for CCZ/T), as shown in Fig. 11B. The obtained results demonstrate that the catalyst stability could be improved by a support. Furthermore, the amount and types of surface mobile oxygen augmented due to the addition of Ce–Zr promoters on the support can effectively suppress catalyst deactivation.

4 Conclusions

Studies on the extensive catalytic performance and structural and surface chemistry properties of Cu–Ce–Zr metal oxides supported on ZSM-5/TiO_2 have been explored in the present study, which reveal the structure-activity relationship in several important aspects:

(1) The catalysts still maintain the structure orderly of ZSM-5/TiO_2 after the addition of copper, cerium and zirconium, and the active CuO species, CeO_2 and ZrO_2 promoters were well dispersed on the supports. The force between the metal oxides

and the support TiO_2 is weaker than that of ZSM-5; moreover, TiO_2 can provide some lattice oxygen.

(2) The low-temperature catalytic activity of ethyl acetate and toluene on CCZ/T was obviously higher than that on CCZ/Z. The larger pore size, more oxygen vacancies and Cu^+ species in CCZ/T are the key factors governing its catalytic activity. The mesopores and macropores in CCZ/T is beneficial for the diffusion of reactants and products. The higher number of oxygen vacancies and Cu^+ species in CCZ/T increases the mobility of atomic oxygen anions can inhibit by-product formation and improve catalytic activity.

(3) It was found that the Mars–van Krevelen mechanism well explained the oxidation reaction. CCZ/Z and CCZ/T showed superior stability for the catalytic removal of ethyl acetate and toluene in 60 h at their complete conversion temperatures and the conversions always remained above 99%, which indicate that the Ce–Zr promoters and optimized support can improve the catalyst stability effectively.

Acknowledgements

We gratefully thank the financial support from the National Natural Science Foundation of China (21307088).

References

1 S. Ojala, S. Pitkäaho, T. Laitinen, N. N. Koivikko, R. Brahmi, J. Gaálová and L. Matejova, *Top. Catal.*, 2011, **54**, 1224–1256.
2 H. Chen, Y. Yan, Y. Shao and H. Zhang, *RSC Adv.*, 2014, **4**, 55202–55209.
3 Y. Z. Wang, S. H. Xie, J. G. Deng, S. X. Deng, H. Wang, H. Yan and H. X. Dai, *ACS Appl. Mater. Interfaces*, 2014, **6**, 17394–17401.
4 M. Konsolakis, A. C. Sónia, B. C. Pedro, L. José and T. Figueiredo, *J. Hazard. Mater.*, 2013, **261**, 512–521.
5 C. He, Y. K. Yu, L. Yue, N. L. Qiao, J. J. Li, Q. Shen, W. J. Yu, J. S. Chen and Z. P. Hao, *Appl. Catal., B*, 2014, **147**, 156–166.
6 J. Sun, L. Bo, L. Yang, X. Liang and X. Hu, *RSC Adv.*, 2014, **4**, 14385–14391.
7 S. A. C. Carabineiro, X. Chen, O. Martynyuk, N. Bogdanchikova, M. Avalos-Borj, A. Pestryakov, P. B. Tavares, J. J. M. Órfão, M. F. R. Pereira and J. L. Figueiredo, *Catal. Today*, 2015, **244**, 103–114.
8 X. Chen, S. A. C. Carabineiroa, S. S. T. Bastosa, P. B. Tavaresb, J. J. M. Órfãoa, M. F. R. Pereiraa and F. Bin, *Appl. Catal., A*, 2014, **472**, 101–112.
9 X. Chen, S. A. C. Carabineiro, P. B. Tavares, J. J. M. Órfãoa, M. F. R. Pereira and J. L. Figueiredo, *J. Environ. Chem. Eng.*, 2014, **2**, 344–355.
10 B. Huang, C. Lei, C. Wei and G. M. Zeng, *Environ. Int.*, 2014, **71**, 118–138.
11 H. M. Xie, X. P. Zhao, G. L. Zhou, X. L. He, H. Lan and Z. X. Jiang, *Appl. Surf. Sci.*, 2015, **326**, 119–123.
12 P. K. Ramaiah, D. Satyasri, S. Sridhar and A. Krishnaiah, *J. Hazard. Mater.*, 2013, **261**, 362–371.
13 L. J. Liu, Z. J. Yao, B. Liu and L. Dong, *J. Catal.*, 2010, **275**, 45–60.
14 L. Y. Lin, C. Y. Wang and H. Bai, *Chem. Eng. J.*, 2015, **264**, 835–844.
15 F. Zhang, F. Jiao, X. L. Pan, K. Gao, J. P. Xiao, S. Zhang and X. H. Bao, *ACS Catal.*, 2015, **5**, 1381–1385.
16 S. Azalim, M. Franco, R. Brahmi, J. M. Giraudon and J. F. Lamonier, *J. Hazard. Mater.*, 2011, **188**, 422–427.
17 S. C. Kim, *J. Hazard. Mater.*, 2002, **91**, 285–299.
18 M. S. Saqer, I. D. Kondarides and E. X. Verykios, *Appl. Catal., B*, 2011, **103**, 275–286.
19 C. He, B. T. Xu, J. W. Shi, N. L. Qiao, Z. P. Hao and J. L. Zhao, *Fuel Process. Technol.*, 2015, **130**, 179–187.
20 C. I. Freitas, S. Damyanova, C. D. Oliveira, C. M. P. Marques and J. M. C. Buenoa, *J. Mol. Catal. A: Chem.*, 2014, **381**, 26–37.
21 M. B. Reddy, P. Lakshmanan and A. Khan, *J. Phys. Chem. B*, 2005, **109**, 1781–1787.
22 G. Postole, B. Chowdhury, B. Karmakar, K. Pinki, J. Banerji and A. Auroux, *J. Catal.*, 2010, **269**, 110–121.
23 W. Tan, G. S. Guo, J. G. Deng, S. H. Xie, H. G. Yang, Y. Jiang and H. X. Dai, *Ind. Eng. Chem. Res.*, 2014, **53**, 18452–18461.
24 T. Tsoncheva, G. Issa, T. Blasco, P. Concepcion and M. Dimitrov, *J. Colloid Interface Sci.*, 2013, **404**, 155–160.
25 F. Bin, X. L. Wei, B. Li and K. S. Hui, *Appl. Catal., B*, 2015, **162**, 282–288.
26 F. Bin, C. L. Song, G. Lv, J. O. Song, S. H. Wu and X. D. Li, *Appl. Catal., B*, 2014, **150–151**, 532–543.
27 S. M. Li, Q. L. Hao, R. Z. Zhao, D. L. Liu, H. Z. Duan and B. J. Dou, *Chem. Eng. J.*, 2016, **285**, 536–543.
28 X. L. Sun, C. R. Gong, G. Lv, F. Bin and C. L. Song, *Mater. Res. Bull.*, 2014, **60**, 341–347.
29 D. Romero, D. Chlala, M. Labaki, S. Royer, J. P. Bellat, I. Bezverkhyy, J. M. Giraudon and J. F. Lamonier, *Catalysts*, 2015, **5**, 1479–1497.
30 J. Wang, L. Deng, D. D. He, J. C. Lu and S. Y. He, *Int. J. Hydrogen Energy*, 2015, **40**, 12478–12488.
31 C. X. Liang, X. Y. Li, Z. P. Qu, M. Tade and S. M. Liu, *Appl. Surf. Sci.*, 2012, **258**, 3738–3743.
32 M. Labaki, J. F. Lamonier, S. Siffert and A. Aboukäıs, *Thermochim. Acta*, 2005, **427**, 193–200.
33 K. N. Renuka, A. V. Shijina, A. K. Praveen and C. U. Aniz, *J. Colloid Interface Sci.*, 2014, **434**, 195–200.
34 J. Brunet, E. Genty, Y. Landkocz, A. M. Zallouha, S. Billet, D. Courcot, S. Siffert, D. Thomas, D. G. Weireld and R. Cousin, *C. R. Chim.*, 2015, **18**, 1084–1093.
35 J. J. Zhu, H. L. Li, L. Y. Zhong, P. Xiao, X. L. Xu, X. G. Yang, Z. Zhao and J. L. Li, *ACS Catal.*, 2014, **4**, 2917–2940.